Vol. 44 (1) (2022) – pp. 63-80 - ISSN: 1012-5965

Delta Journal of Science

Available online at **https://djs.journals.ekb.eg/**

Research Article

GEOLOGY

Petrophysical Evaluation Using Well Logging of the Alam El-Beuib Reservoirs, Shushan Basin, North Western Desert, Egypt

I. Othman*[1], A. Abdeldayem[1], and M.R. Soliman[1], G. El-Qady[2]

[1]Geology Department, Faculty of Science, Tanta University, Tanta 31527, Egypt

[2]National Research Institute of Astronomy and Geophysics (NRIAG), Helwan, Egypt

***Corresponding author:** *Ibrahim Othman* **E-mail:** *ibrahim.othman@science .tanta.edu.eg*

Received: 26/12/2022 Accepted : 20/1/2022

KEY WORDS

Alam El-Buieb Reservoir; well logs; petrophysical evaluation; Shushan basin; North Western Desert.

ABSTRACT

Petrophysical analysis of some of the Lower Cretaceous Alam El-Bueib reservoir units were carried out using wireline logs from four wells representing two fields (GEB and APRIES) located in the western part of the Shushan Basin, north Western Desert. Several petrophysical parameters were calculated and used in the subdivision of the studied reservoirs, including shale volume (V_{SH}), total and effective porosities (PHI_T, PHI_E), water saturation (S_W), and hydrocarbon saturation (S_H). Neutron versus density and M-N crossplots indicated that quartzose sandstone is the major matrix component with minor carbonates in some units. Furthermore, the litho-saturation crossplots indicated the existence of oil-bearing intervals, which are frequently associated with quartzose sandstones with low silt and clay content. Dispersed and laminated clays are detrimental to reservoir quality as they block pore spaces, decreasing hydrocarbon storage and flow capacities. Analysis of petrophysical data shows that the studied units have a good reservoir quality, with effective porosity values between 8 and 10 % with an average value 9% and low water saturation values of less than 35%. The most prospective reservoir intervals are found in the upper and middle reservoir units and are recommended for future exploration and development.

1. Introduction

The Shushan basin **(Fig. 1)** represents one of Egypt's most productive petroleum provinces in the north Western Desert. This study targets some reservoir parts of the Alam El-Buieb (AEB) Formation including AEB-3D, AEB-3G, and AEB-6 units with their known high hydrocarbon potentiality (**EGPC, 1992)**. The main purposes of this study are to evaluate the reservoir characteristics of the concerned units through the identification of their lithology, fluid saturation, and porosity, as well as to define cutoffs and identify the pay zones using various reservoir parameters, hence their hydrocarbon potentiality.

2. Geologic setting

Geological and drilling studies in the Shushan basin revealed the presence of a dense subsurface lithostratigraphic column, varying in age from the Paleozoic to the Recent **(Fig. 2)**. The post-Paleozoic succession includes four main cycles of tectono-sedimentary sequences distinguished by unconformities, crossing to the Middle Jurassic, Lower Cretaceous, Upper Cretaceous, and Eocene to Miocene. Each of these cycles starts with fluvio-deltaic siliciclastics and ends with marine carbonates **(Sultan and Abdelhalim, 1988; May, 1991; EGPC, 1992; Shalaby *et al.*, 2013a)**. The north Western Desert, where the study area is located, was initially formed mainly due to vertical movement of basement blocks that are dominated by parallel, elongated, tilted fault blocks, producing horst and half-graben structures associated with the erosion of the upthrown blocks (**Shalaby *et al.*, 2013b; Barakat, 2017; Mahmoud *et al.*, 2019**).

Shushan basin is situated within the tectonic zone of the unstable shelf that had been active throughout most of the Paleozoic to Early Cenozoic times, where the Late Jurassic to Early Cretaceous rifting, Mid-Cretaceous (Aptian) uplift and erosion, and the Late Cretaceous to Early Tertiary shear and compression took place (**Said, 1962; Marfil *et al.*, 2003**). During the Late Jurassic- Early Cretaceous, Shushan basin was formed as a sequence of opening of Neo-Tethys ocean to the north as a NE- SW extensional basin, receiving only continental and fluvio-lacustrine sediments and later converted into a pull-apart basin during the Late Cretaceous as a result of the rifting of the North African plate from the Eurasian plate **(Meshref and Hammouda, 1990; EGPC, 1992; Meshref, 1996; Metwalli and Pigott, 2005; Al-Sharhan and Abd El- Gawad, 2008; Hakimi *et al.*, 2012; Barakat, 2017)**.

3. Materials and Methods

This study is based on well log data from four wells (GEB-1X, GEB-2X, SHU-1X, and APRIES-1X) representing two fields (GEB and APRIES) located in the western part of the Shushan Basin, north Western Desert. The well log evaluation has been accomplished using Interactive Petrophysics software (IP) version 3.5. Well log data include gamma-ray, resistivity, sonic, neutron, and density, were used to identify lithology and fluid type and determine shale volume, total porosity, effective porosity, water, and hydrocarbon saturation.

3.1. Density - Neutron and M – N Crossplots

Crossplots of binary porosity logs are useful in displaying both porosity and lithology parameters using combined bulk density (RHO_B) and neutron porosity (N_{PHI}) values. Points relating to certain water-

saturated, pure lithology form lines (quartz, limestone, dolomite, etc.).

When the matrix lithology is a binary combination (quartz-lime or lime-dolomite), the point drawn from the log values will lie between the lithology lines**.** The influence of shale may also be seen on the crossplot, where shale effects tend to be concentrated in the southeast quadrant of the crossplot (**Poupon and Leveaux, 1971**).

The use of M-N cross-plots improves mineralogical interpretation by utilizing of neutron, density, and sonic logs data (**Bruke *et al*., 1969)**. These graphs incorporate the lithology-dependent variables M and N from all three porosity logs: sonic, neutron, and density (**Schlumberger, 1989**).

The following equations are used to compute M and N values (**Schlumberger, 1972**):

$$M = (\Delta t_f - \Delta t) / (\rho b - \rho b_f) \times 0.01 \quad (1)$$

$$N = (\Phi N_f - \Phi N) / (\rho b - \rho b_f) \quad (2)$$

3.2. Shale volume calculation

Accurate estimation of the shale volume is essential for the petrophysical evaluation of clastic reservoir rocks. Shale volume calculation is crucial for eliminating the effect on logging responses and discriminating between the reservoir and non-reservoir rock. Gamma-ray, resistivity, neutron, and neutron-density logs were used to calculate the shale volume. The average value of shale content from these methods is approximately equal to its actual value (**Hakimi *et al*., 2012**). Neutron-density crossplot as well as shale volume-porosity crossplot were used to trace the distribution and define the type of shale and its effect on reducing the pore space (**Thomas and Stieber, 1975**).

Following Khalda Petroleum Company Internal Report (2014), the cutoff value of shale in the study area is 40%, meaning rocks with more than 40% of shale content are considered non- reservoirs, while those with less than 40% of shale content are regarded as a reservoir**.**

3.3. Porosity calculation

Neutron, density, and sonic logs are commonly used to calculate pore volume within the rocks. Neutron log is directly related to fluids fully occupying the pore space (porosity), density log is a function of the density of the matrix, porosity, and the density of the fluid in pores, while the sonic log is related to the clean compacted rocks (primary porosity). Total and effective porosities (PHI_T and PHI_E) are calculated using the neutron density- initial porosity model (**Asquith and Gibson, 1982**). Neutron density porosity- sonic porosity crossplot is used to identify the porosity type.

Determination of density porosity is conducted by using this formula **(Schlumberger, 1974)**

$$\phi_D = (\rho b_{ma} - \rho b_{log}) / (\rho b_{ma} - \rho b_f) \quad (3)$$

The matrix density (**Table 1**) and type of fluid in the borehole must be known (**Asquith and Gibson, 1982**).

Determination of neutron porosity is conducted by using this formula (**Schlumberger, 1972**):

$$(\Phi_N)c = \Phi_N - (V_{sh} \times (\Phi_N)_{sh}) \quad (4)$$

The combination of the density porosity $(\Phi_D)_C$ and neutron porosity $(\Phi_N)_C$ is useful to obtain the effective porosity, where a comparison is made between them. In zones of $(\Phi_N)_C$ greater than $(\Phi_D)_C$, the following formula is applied **(Gaymard and Poupan, 1968)**:

$$\phi_{eff} = (\phi_{Nc} + \phi_{Dc}) / 2 \quad (5)$$

When the formation contains gas, $(\Phi_D)_C$ will be greater than $(\Phi_N)_C$ and the effective porosity can be calculated using

the following equation **(Gaymard and Poupan, 1968)**:

$$(\phi_{eff})^2 = (\phi_{Nc}^2 + \phi_{Dc}^2) / 2 \quad (6)$$

Following **Khalda Petroleum Company Internal Report (2014)**, an 8% porosity cutoff, considered the lowest effective porosity that allows oil to flow, is applied to differentiate between porous and non-porous sand intervals.

3.4. Fluid saturation

Archie equation is used to calculate the water saturation as it defines the shale effect for the clean formation (Archie's term).

All water saturation determinations from resistivity logs in the uninvaded zone with a homogeneous intergranular porosity are calculated using the following **Archie's (1942)** formula:

$$S_w^n = (F \times R_w) / R_t \quad (7)$$

F is usually obtained from the measured porosity of the formation through the following relations:

$$F = a / \phi^m \quad (8)$$

Where, (m) and (a) are constantly determined from local experience.

The most common values for (a) and (m) are as follows:

For Sandstone **a = 0.62 & m = 2.15 (Winsauer *et al.*, 1952)** (9)

or **a = 0.81 & m = 2.0 (Schlumberger, 1972)** (10)

For Limestone **a = 1.0 & m = 2.0 (Carthers, 1968)** (11)

The hydrocarbon saturation is calculated using the following equation (**Rider, 1996**):

$$S_h = (1 - S_w) \quad (12)$$

Where S_h is the hydrocarbon saturation and S_w is the water saturation.

Following **Khalda Petroleum Company Internal Report (2014)**, a 50% water saturation cutoff is used to differentiate between the pay and non-pay zones.

4. Results and Interpretation

4.1. Discrimination of reservoir lithologies

The studied Alam El-Bueib reservoir units are composed primarily of white to yellow sandstones, with siltstones and grey shales as minor constituents. Thin carbonate layers (limestone and dolomite) occurred in most areas. Carbonates become more abundant towards the top. Dolomite and oolitic limestone layers increase in thickness to the northwest (**RRI Robertson, 1982**). The interpretation of the lithology of the reservoir zones within the formation revealed that, the predominant lithology is sandstone with some carbonates in the four studied wells.

4.1.1 AEB-3D Reservoir

Analysis of petrophysical parameters in the studied wells (**Table 2**) revealed that this unit is regarded as a reservoir in GEB-1X, SHU-1X, and APRIES-1X wells but not in GEB-2X well, hence neutron-density and M-N crossplots were not constructed for this well.

Figure 3 shows the neutron-density crossplots for this reservoir unit. The plots lie around the sandstone line for both GEB-1X and SHU-1X wells with porosity range of 5-7% and 7-12% respectively, indicating that sandstone form the main lithology of this unit in these two wells. As for the APRIES-1X well, the plots fall between the sandstone and limestone lines, with an average porosity range of 7-10%, indicating that both lithologies form this unit.

Figure 4 shows the M-N cross-plots for this reservoir unit. Plots from both GEB-1X and SHU-1X wells are scattered around the quartz sandstone line, indicating the abundance of clean quartzose sandstones in

this reservoir unit. As for the APRIES-1X, the points are scattered in the area between the quartz sandstone and calcite lines, indicating the predominance of sandstone with carbonate cement.

4.1.2 AEB-3G Reservoir

Analysis of petrophysical parameters in the studied wells (**Table 3**) revealed that this unit is regarded as a reservoir in the GEB-2X, SHU-1X, and APRIES-1X wells. This unit does not exist in the GEB-1X well due to local faulting (**Khalda Petroleum Company's internal report, 2014).**

Figure 5 shows the neutron-density crossplots for this reservoir. The plots lie around the sandstone line for both GEB-2X and APRIES-1X wells with porosity ranges of 5-7% and 5-10%, respectively, indicating that sandstone forms this unit's main lithology in these two wells**.** As for the SHU-1X well, the plots fall on the sandstone and limestone lines, with an average porosity range of 4-10%, indicating that both lithologies form this unit.

M-N crossplot is not constructed for this reservoir unit in GEB-2X well as there is no sonic log data available for this well (**Khalda Petroleum Company internal report, 2014)**

Figure 6 shows the M-N cross-plots for this reservoir unit in APRIES-1X and SHU-1X wells. Plots from the APRIES-1X well are scattered around the quartz sandstone line, indicating this reservoir unit's abundance of clean quartzose sandstones. As for the SHU-1X well, the points are scattered in the area between the quartz sandstone and calcite lines, indicating the predominance of sandstone with carbonate cement in this reservoir unit.

4.1.3 AEB-6 Reservoir

Analysis of petrophysical parameters in the studied wells **(Table 4)** revealed that this unit is regarded as a reservoir in both the GEB-1X and GEB-2X wells but not in SHU-1X and APRIES-1X wells.

Figure 7 shows the neutron-density crossplots for this reservoir unit in GEB-1X and GEB-2X wells. The plots lie around the sandstone line for GEB-1X well with porosity range of 5-10%, indicating that sandstone forms the main lithology of this unit in this well. As for the GEB-2X well, the plots fall along the sandstone and limestone lines, with an average porosity range of 4-7%, indicating that both lithologies form this unit.

M-N crossplot is not constructed for GEB-2X well as the sonic log was not conducted in this well (**Khalda Petroleum Company internal report, 2014)**

Figure 8 shows the M-N cross-plots for this reservoir unit. Plots from GEB-1X well are scattered in the area between the quartz sandstone and calcite lines, indicating the predominance of sandstone with carbonate cement for this reservoir unit.

4.2. Petrophysical evaluation of the Alam El-Buieb units

Tables 2, 3, and 4 summarize the values of different petrophysical parameters of the studied AEB three reservoir units. The following sections detailed the analysis of these parameters and interpretation in terms of reservoir quality**.**

4.2.1 Litho-saturation crossplots of AEB-3D unit

Analysis of litho-saturation crossplot of AEB – 3D Unit in GEB – 1X well **(Fig. 9)** indicates the presence of mixed lithology of sandstone, shale, and limestone with an increase of shale at some intervals at the middle part of the unit. Sandstone alternates with shale and limestone that appears as thin laminae intercalated with shale through the whole unit. Analysis of porosity and hydrocarbon saturation results indicates the presence of few reservoir intervals in the

lower part of the unit, especially, where shale content is high (up to 85%).

Analysis of litho-saturation crossplot of this unit in GEB – 2X well **(Fig. 10)** reflects a mixed lithology of shale, sandstone, and limestone with shale as the predominant lithology. Sandstone alternates with shale and limestone that appears as thin laminae intercalated with shale through the entire unit. Analysis of porosity and hydrocarbon saturation results shows that this unit could not be a reservoir as shale content is high at most unit parts (80%)**.**

Analysis of litho-saturation crossplot of this unit in SHU–1X well **(Fig. 11)** indicates the presence of mixed lithology of sandstone, shale, and limestone with sandstone dominating while shale alternates with sandstone and limestone that appears as thin laminae throughout the entire unit. Analysis of porosity and hydrocarbon saturation results shows the presence of reservoir and pay interval in the middle part of the unit that is represented by a large sand body, where maximum shale content is low and don't exceed 4%. Effective porosity is about 9% and water saturation is 38%.

Analysis of litho-saturation crossplot of this unit in APRIES– 1X well **(Fig. 12)** reflects a mixed lithology of sandstone, shale, and limestone with shale increasing at some intervals, especially, towards the lower part of the unit. The sandstone is found only at the upper part of the unit, while limestone appears as thin laminae intercalated with shale throughout the entire unit. Analysis of porosity and hydrocarbon saturation results shows the presence of reservoir and pay interval in the upper part of the unit where the shale content is about 4%, water saturation is 25%, and effective porosity is 9%.

4.2.2 Litho-saturation crossplots of AEB-3G Unit

Analysis of the log data of the AEB-3G unit shows absence of this unit in GEB-1X well probably due to local faulting **(Khalda Petroleum Company Internal Report, 2014)**.

Analysis of litho-saturation crossplot of this unit in GEB – 2X well **(Fig. 10)** reflects a mixed lithology of sandstone and limestone. Sandstone is predominant in the upper and lower parts of the unit with alternates of limestone that appears as thin laminae at the middle part. Analysis of porosity and hydrocarbon saturation results shows the presence of reservoir zones in many parts of the unit, where shale content is low (reaching 3 - 6%) and effective porosity averages 7.5%. The upper part is evaluated as a pay zone where water saturation reaches 35–45%.

Analysis of litho-saturation crossplot of this unit in SHU–1X well **(Fig. 11)** reflects that sandstone is the predominant lithology with very thin laminae of shale only at the middle part of the unit. Analysis of porosity and hydrocarbon saturation results shows the presence of reservoir and pay interval in the middle part of the unit, where maximum shale content is low (< 1.7%), effective porosity is about 9%, and water saturation reaches 30%.

Analysis of litho-saturation crossplot of this unit in APRIES–1X well **(Fig. 12)** reflects that sandstone is the predominant lithology with some thin laminae of shale, especially, in the upper part of the unit. Analysis of porosity and hydrocarbon saturation results shows the presence of some reservoir intervals at the lower part of the unit where shale content is low reaching 3-4%, water saturation 70- 85%, and effective porosity of 8 -12%.

4.2.3 Litho-saturation crossplots of AEB-6 unit

Analysis of litho-saturation crossplot of this unit in GEB–1X well **(Fig. 13)** indicates the presence of mixed lithology of sandstone, shale, and limestone. Sandstone alternates with shale in the upper part of the section but shale increases at some intervals at the lower part of the unit while sandstone alternates with shale and limestone that appears as thin laminae intercalated with shale throughout the entire unit. Analysis of porosity and hydrocarbon saturation results shows the presence of some reservoir intervals in the upper part of the unit where shale content is low and don't exceed 5%, effective porosity is about 9% and water saturation reaches 80%, except for a zone in the upper part that represents a pay zone where water saturation reaches 23%.

Analysis of litho-saturation crossplot of this unit in GEB–2X well **(Fig. 14)** reflects a mixed lithology of sandstone, shale, and limestone. Sandstone predominates in the middle part of the unit with some alternating shale intervals which increase at the upper and lower parts where limestone appears as thin laminae intercalated with shale throughout the entire unit. Analysis of porosity and hydrocarbon saturation results shows the presence of some reservoir and pay intervals in the middle part of this unit where maximum shale content is low and doesn't exceed 7%, effective porosity is about 7.5%, and water saturation reaches 10 - 13%.

Analysis of litho-saturation crossplot of this unit in SHU–1X well **(Fig. 15)** reflects a mixed lithology of limestone and shale. The limestone is predominant in the upper and lower parts of the unit with alternates of shale that appear as thin laminae at the middle part of the unit where high proportions of shale volumes may reach 65% at some intervals. Analysis of porosity and hydrocarbon saturation results shows that this unit is not considered as a reservoir, as shale content is high in most parts of the unit reaching 85% and effective porosity is around 0%.

Analysis of litho-saturation crossplot of this unit in APRIES–1X well **(Fig. 16)** reflects a mixed lithology of shale and limestone. Shale is predominant in this unit with limestone alternations that appear as very thin laminae at the lower part of the unit. Analysis of porosity and hydrocarbon saturation results shows that this unit is not considered as a reservoir as shale content is high in most parts reaching 80- 95% with effective porosity around 0%.

5. Conclusion

The petrophysical properties of the Lower Cretaceous Alam El-Bueib AEB-3D, AEB-3G, and AEB-6 reservoir units in the western part of Shushan basin have been evaluated using a complete wireline log set from four wells (GEB-1X, GEB-2X, SHU-1X APRIES-1X). Density - Neutron and M-N crossplots have revealed that the lithology of studied units is dominated by mixed lithology of sandstones with shale and limestone. Sandstones are of a quartzose type with carbonate cement with good petrophysical properties in terms of effective porosity and fluid saturation. Shale is distributed in the sand as laminated intercalations causing the pore volume to be at its minimal levels. In contrast, dispersed shale largely decreases the pore volume and increases water saturation most probably due to their high contents of irreducible water saturation. High porosity in these units is mainly present in the quartzose and calcareous sandstones. Hydrocarbon pay zones with low water saturation values (less than 50%) often occupy the upper and middle parts of the

different units where the sandstones are dominant. Future exploration in the study area should target the sandstone zones which are commonly present at the top and middle parts of the studied three reservoir units.

Acknowledgments

Deep gratitude and sincere appreciation to the Egyptian Petroleum Corporation (EGPC) and Exploration Management of Khalda Petroleum Company (KPC) for providing well data used in this study. This study has benefited from constructive discussions with keen KPC staff **Dr. Abdelmoniem Abo Shady**, Geological Operation General Manager, **Dr. Mohamed Elbastawessy**, Assistant General Manager of Petrophysics Department, **Dr. Mohamed Sobhy**, Assistant General Manager of Prospect, **Mr. Mohamed Elsawy**, Petrophysical Operation Department Head, **Mr. Islam Abbas**, Prospect Generation Department Head.

References

Al-Sharhan, A.S., Abd El-Gawad, E.A., 2008. Geochemical characterization of potential Jurassic/ Cretaceous source rocks in the Shoushan Basin, north Western Desert, Egypt. *J. Petrol. Geol.* 31: 191-212.

Archie, G. E., 1942. The electrical resistivity log as an aid in determining some reservoir characteristics; Trans; AIME, 146: 54-62.

Asquith, G.B., and Gibson, C.R., 1982. Basic Well Log Analysis for Geologists. The AAPG, Tulsa, Oklahoma, USA, 216p.

Barakat, M.K., 2017. Petrophysical Evaluation and Potential Capability of Hydrocarbon Generation of Jurassic and Cretaceous Source Rocks in Shoushan Basin, North Western Desert, Egypt. IOSR *J. App. Geol. and Geoph*., 5: 23-45.

Burke, J., Campbell Jr., R. and Schmidt, A., 1969. The litho-porosity cross plot a method of determining rock characteristics for computation of log data. Presented at SPWLA tenth annual logging symposium, May 25-28 and the SPE Illinois Basin Regional Meeting, Evansville, Indiana, 30-31 October. SPE-2771-MS.

Carthers, J.W., 1968. A statistical study of the formation factor relationship. The Log Analyst, 9: 14-20.

EGPC, 1992. Western Desert, oil and gas fields, a comprehensive overview. 11th Egyptian General Petroleum Corporation Exploration and Production Conference, Cairo, pp. 1-431.

Gaymard, R., and Poupan, A., 1968. Response of neutron and formation density logs in hydrocarbon-bearing formations. The log Analyst, 5: 3-12.

Hakimi, M.H., Shalaby, M.R., and Abdullah, W.H., 2012. Diagenetic characteristics and reservoir quality of the Lower Cretaceous Biyadh sandstones at Kharir oilfield in the western central Masila Basin, Yemen. *J. Asian Earth Sci.,* 5: 109–120.

Khalda Petroleum Company Internal Report, 2014. Petrophysical and final geological report from GEB and APRIES fields, Western Desert, Egypt.

Mahmoud, M.S., Deaf, A.S., Tamam, M.A., and Khalaf, M.M., 2019. Revised (microspores-based) stratigraphy of the Lower Cretaceous succession of the Minqar-IX well, Shushan Basin, north Western Desert, Egypt: Biozonation and correlation approach. *J .African Earth Sci*., 151 :18-35.

Marfil, R., Delgado, A., Rossi, C., and Ramseyer, K., 2003. Origin and Diagenetic Evolution of Kaolin in Reservoir Sandstones and Associated Shales of the Jurassic and Cretaceous, Salam Field,

Western Desert, Egypt. International Association Sedimentology, 34: 319-342.

May, R.M., 1991. The Eastern Mediterranean Mesozoic Basin: evolution and oil habitat. AAPG Bulletin, 75: 1215–1223.

Meshref, W.M., 1996. Cretaceous tectonics and its impaction on oil exploration in Regional Northern Egypt. Geological Society, Egypt, 2: 199- 241.

Meshref, W.M., and Hammouda, H., 1990. Basement tectonic map of Northern Egypt. Proceedings of the EGPC 9th Exploration and Production Conference, Cairo. Egyptian General Petroleum Corporation Bulletin, 1: 55–76.

Metwalli, F.I., and Pigott, J.D., 2005. Analysis of petroleum system criticals of the Matruh–Shushan Basin, Western Desert, Egypt. Petroleum Geoscience, 11: 157- 178.

Poupon, A., and Leveaux, J., 1971: Evaluation of water saturation in shaly Formations, The Log Analyst, 12: 3-8.

Rider, M. H., 1996. The Geological Interpretation of Well Logs. Rider-French Consulting Ltd, Sutherland, Scotland, 280 p.

Robertson Research International (RRI), 1982. Petroleum Potential Evaluation, Western Desert, the Arab Republic of Egypt. Report and Enclosures, 7 Vols, 220p.

Said, R., 1962. The Geology of Egypt. Amsterdam. New York: Elsevier Publishing Company, 377p.

Schlumberger, 1972. The essential of log interpretation practice. Schlumberger Ltd., France, pp. 45-67.

Schlumberger, 1974. Log interpretation manual/application. vol. 2 Houston, Schlumberger well services, Inc., 435 p.

Schlumberger, 1989. Log Interpretation Principles/Applications, 228p.

Schlumberger, 1995. Well Evaluation Conference, Egypt. Schlumberger Technical Editing Services, Chester. pp. 58-66.

Shalaby, M.R., Hakimi, M.H., and Abdullah, W.H., 2013a. Organic geochemical characteristics and interpreted depositional environment of the Khatatba Formation, north Western Desert, Egypt. AAPG Bulletin, 96: 2019-2036.

Shalaby, M.R., Hakimi, M.H., and Abdullah, W.H., 2013b. Modeling of gas generation from the Alam El-Bueib formation in the Shoushan Basin, north Western Desert of Egypt. *Int. J. Earth Sci.* (GeolRundsch), 102: 319-332.

Sultan, N., and Abdelhalim, M., 1988. Tectonic framework of north Western Desert, Egypt and its effect on hydrocarbon accumulation, 9th Explo. Conf., EGPC, Cairo, Egypt, p31.

Thomas, E.C., and Stieber, S.J., 1975. The distribution of shale in sandstones and its effect on porosity. In: Trans. SPWLA 16th Annual Logging Symposium, New Orleans, Louisiana.

Wescott, W.A., Atta, M., Blanchard, D.C., Georgeson, S.T., Miller, D.A., Walter, W.O., Welson, AD, Dolson, J.C., Sehim, A., 2011. Jurassic rift Architecture in the Northeastern Western Desert, Egypt. AAPG international conferecnce and exhibition, Milan, Italy, October 23-26.

Winsauer, H. M., 1952. Resistivity of Brine–Saturated Sands in Relation to Pore Geometry, AAPG Bulletin, 36: 253-277.

.

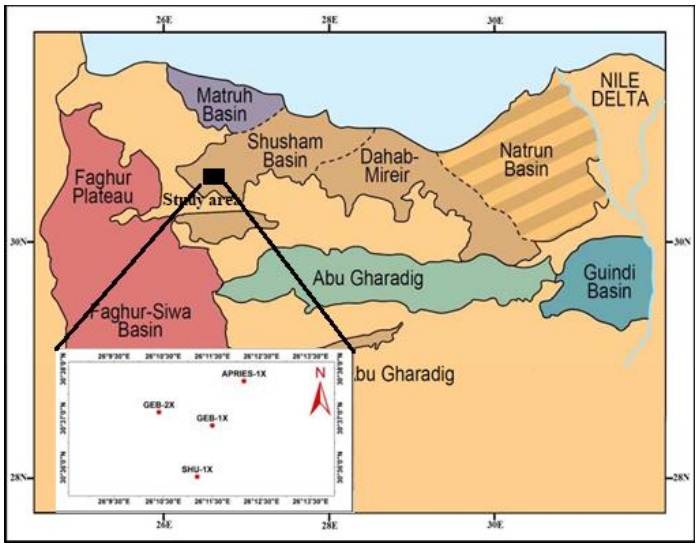

Fig.1. Western Desert basins delineation map **(Schulmberger, 1995)** and location of the study area.

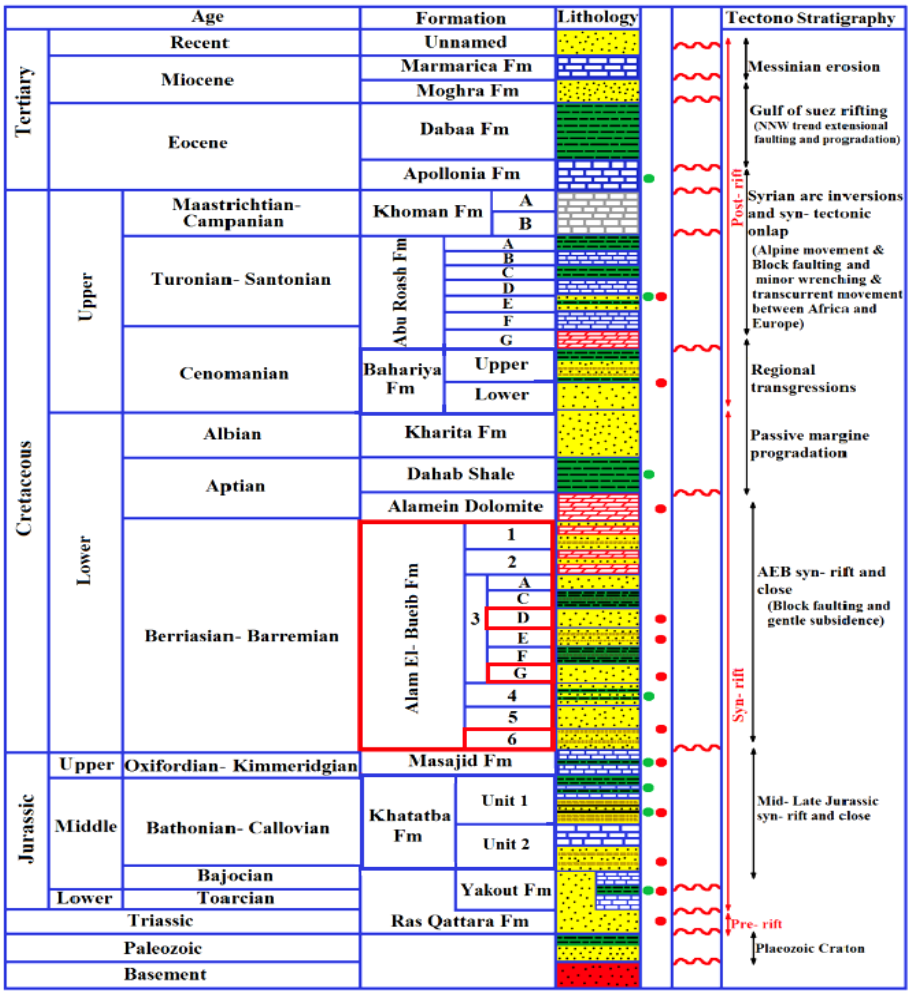

Fig. 2. Generalized lithostratigraphic column of the Shushan basin (**Wescott *et al*., 2011**).

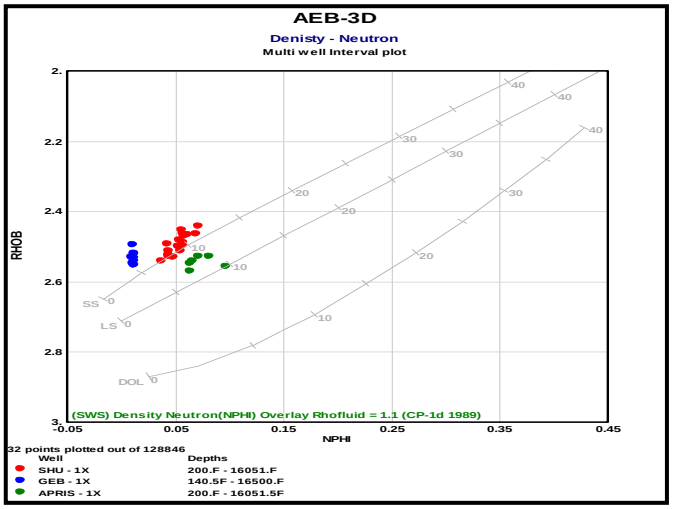

Fig. 3. Density-Neutron cross-plot of AEB-3D reservoir in the study area.

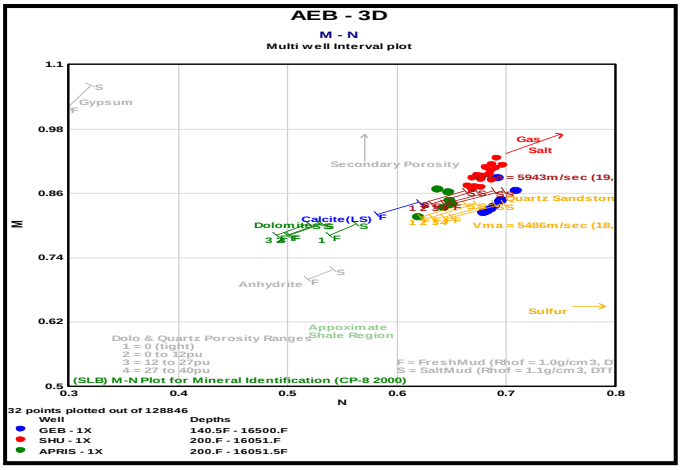

Fig. 4. M-N cross-plot of AEB-3D reservoir in the study area.

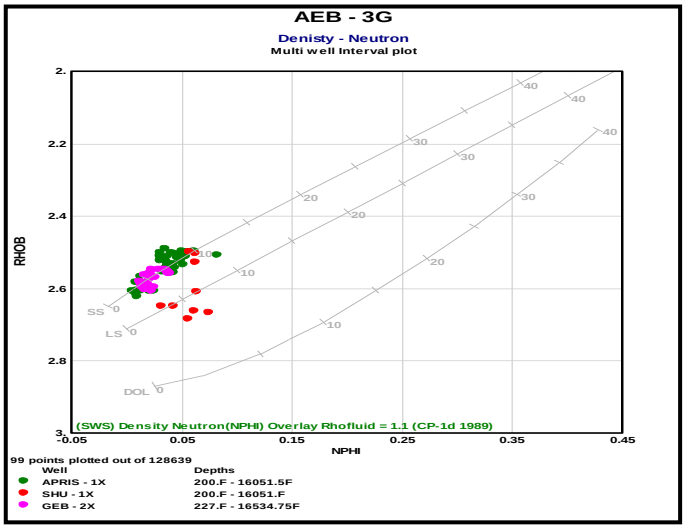

Fig. 5. Density-Neutron cross-plot of AEB-3G reservoir in the study area.

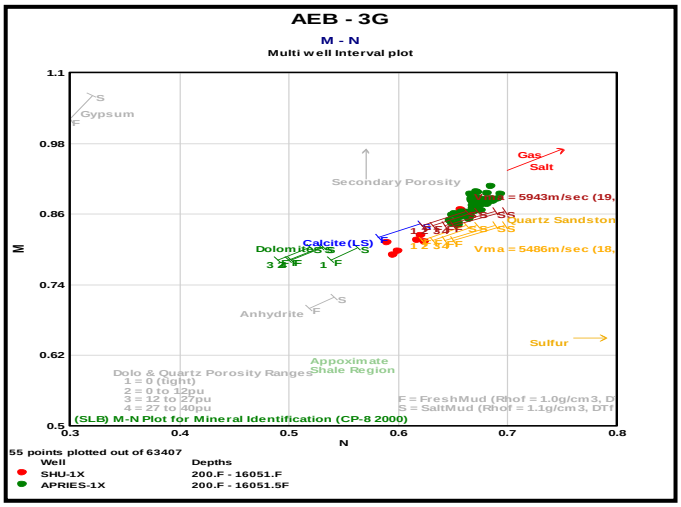

Fig. 6. M-N cross-plot of AEB-3G reservoir in the study area.

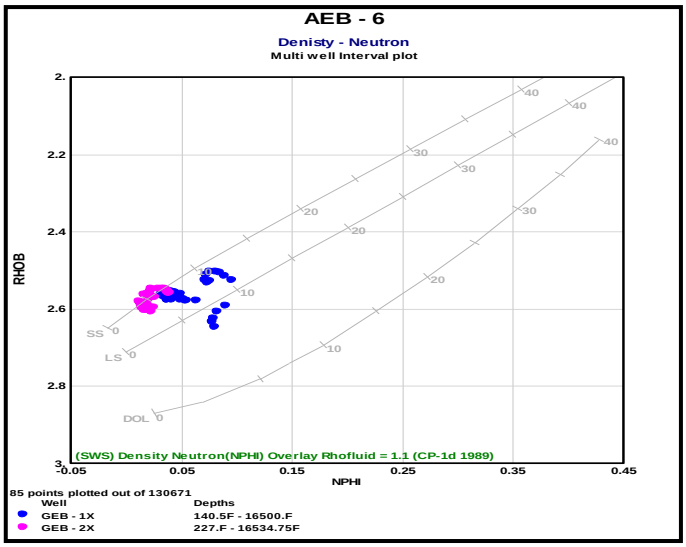

Fig. 7. Density-Neutron cross-plot of AEB-6 reservoir in the study area.

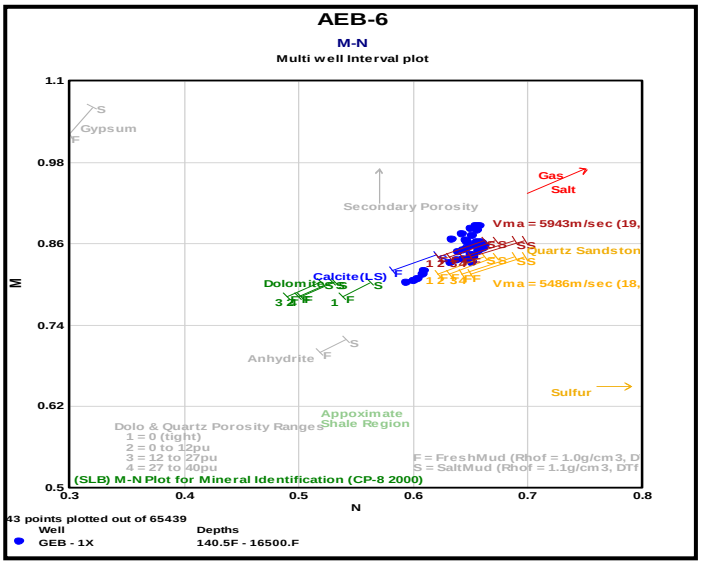

Fig. 8. M-N cross-plot of AEB-6 reservoir in the study area.

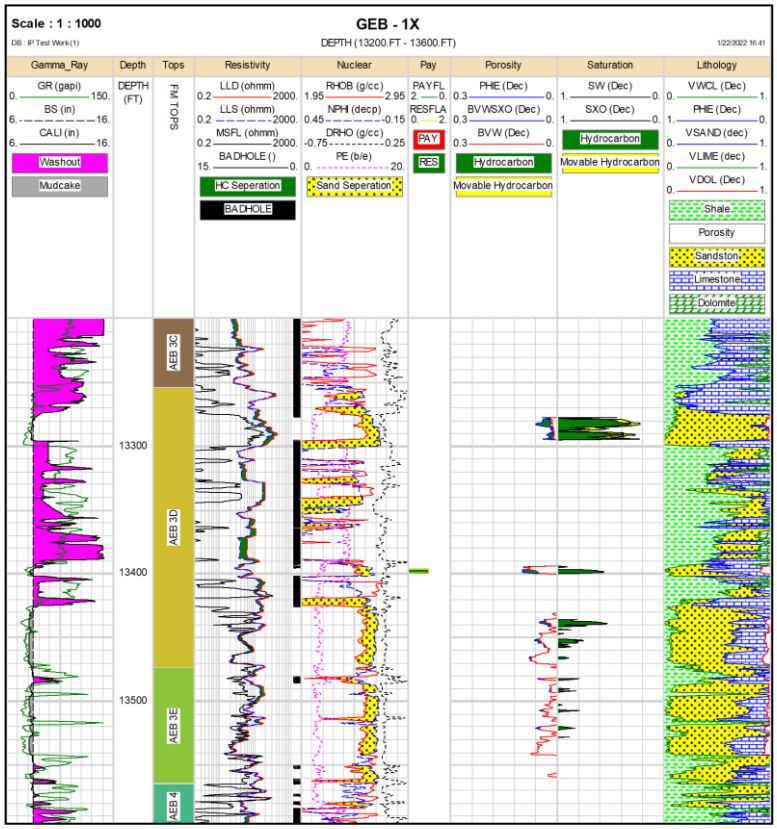

Fig.9. Litho-Saturation Crossplot of AEB-3D unit in GEB-1X well.

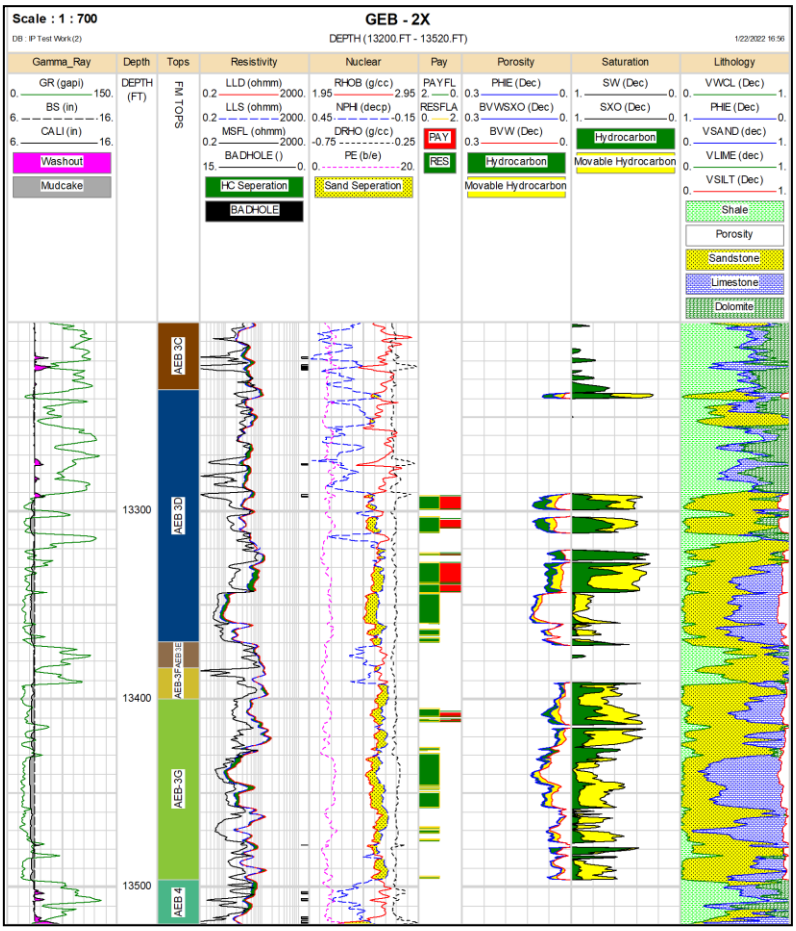

Fig.10. Litho-Saturation Crossplot of AEB-3D and 3G units in GEB-2X well

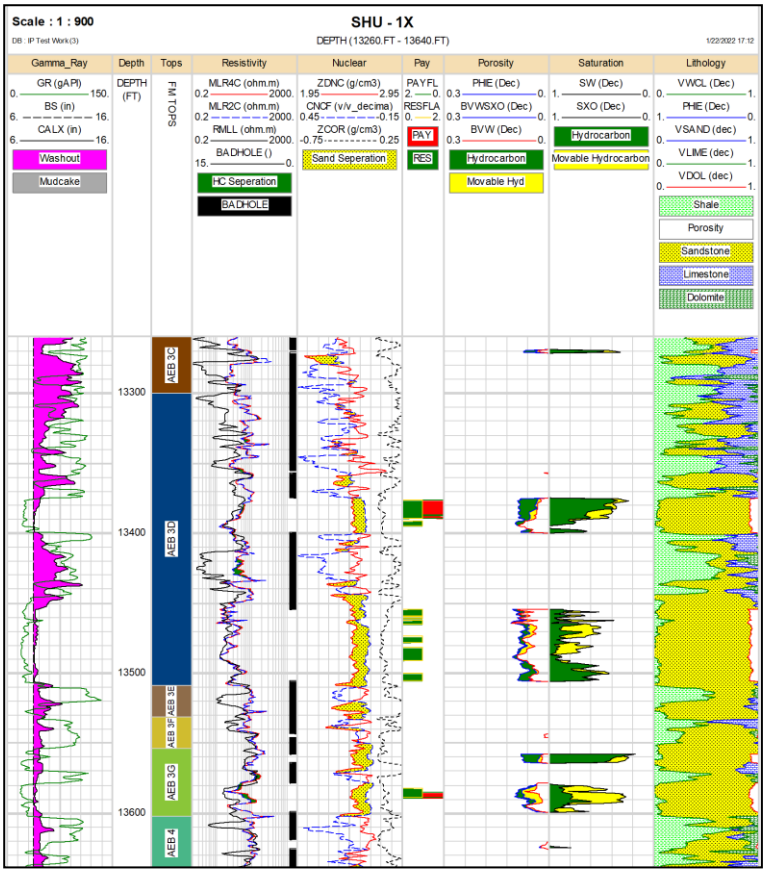

Fig.11. Litho-Saturation Crossplot of AEB-3D and 3G units in SHU-1X well

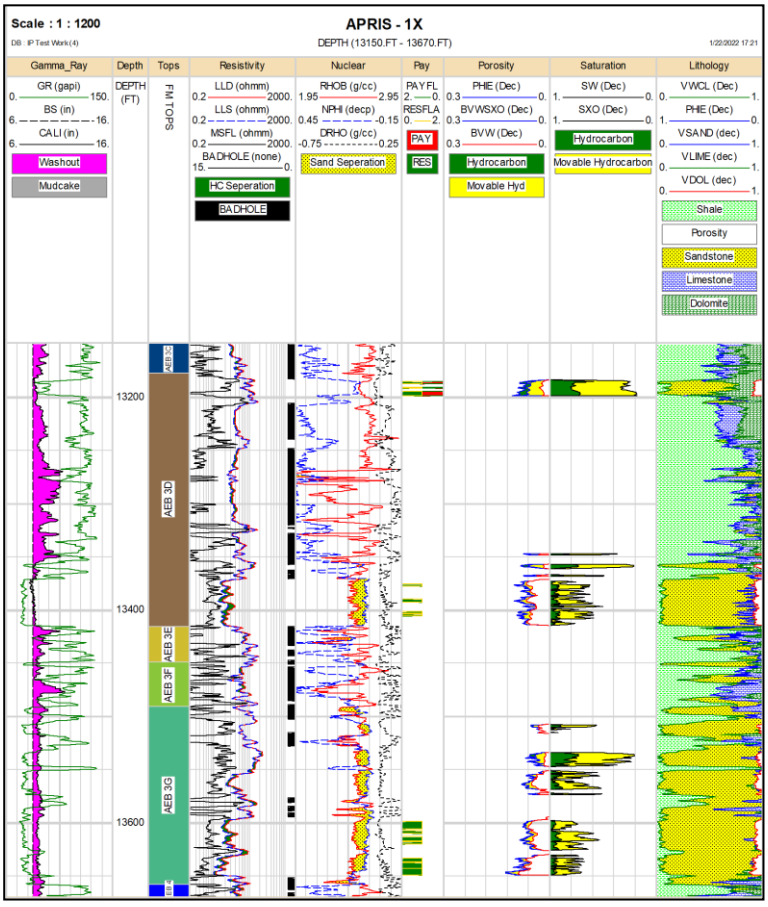

Fig.12. Litho-Saturation Crossplot of AEB-3D and 3G units in APRIES-1X well.

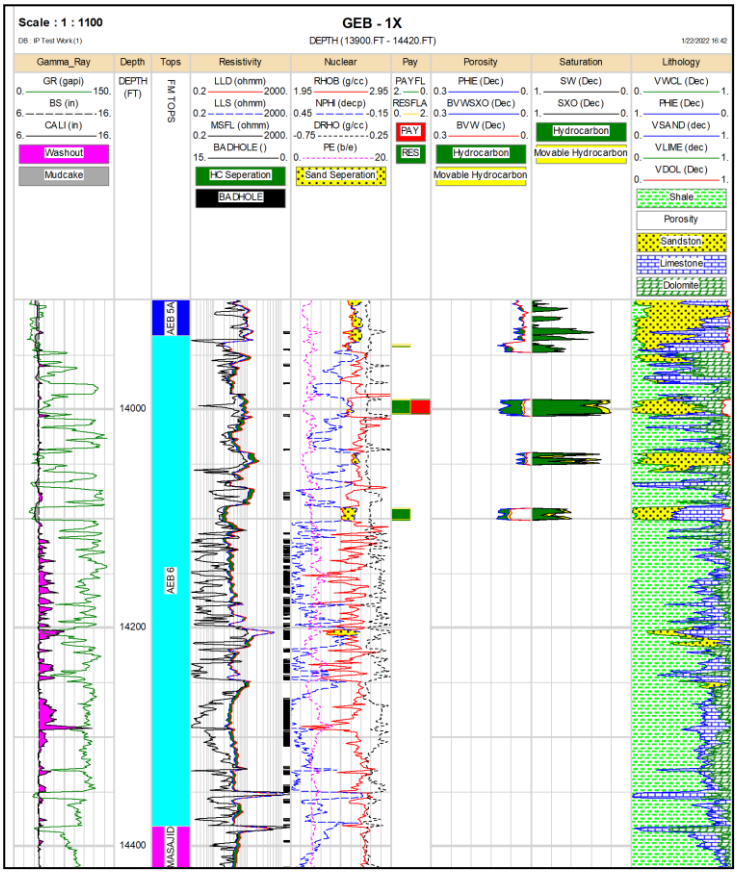

Fig.13. Litho-Saturation Crossplot of AEB-6 unit in GEB-1X well.

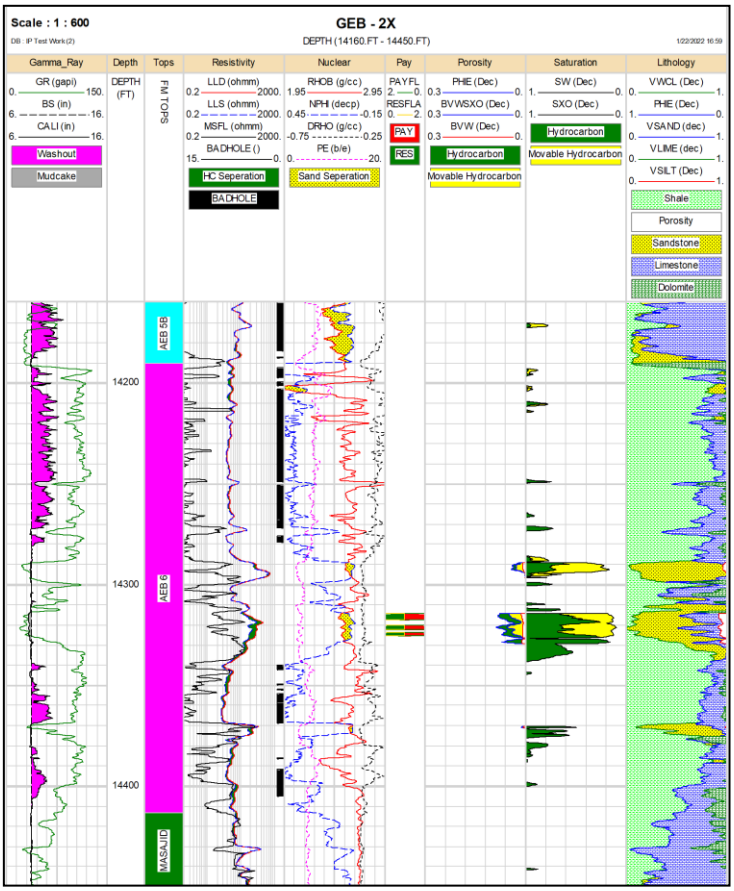

Fig.14. Litho-Saturation Crossplot of AEB-6 unit in GEB-2X well.

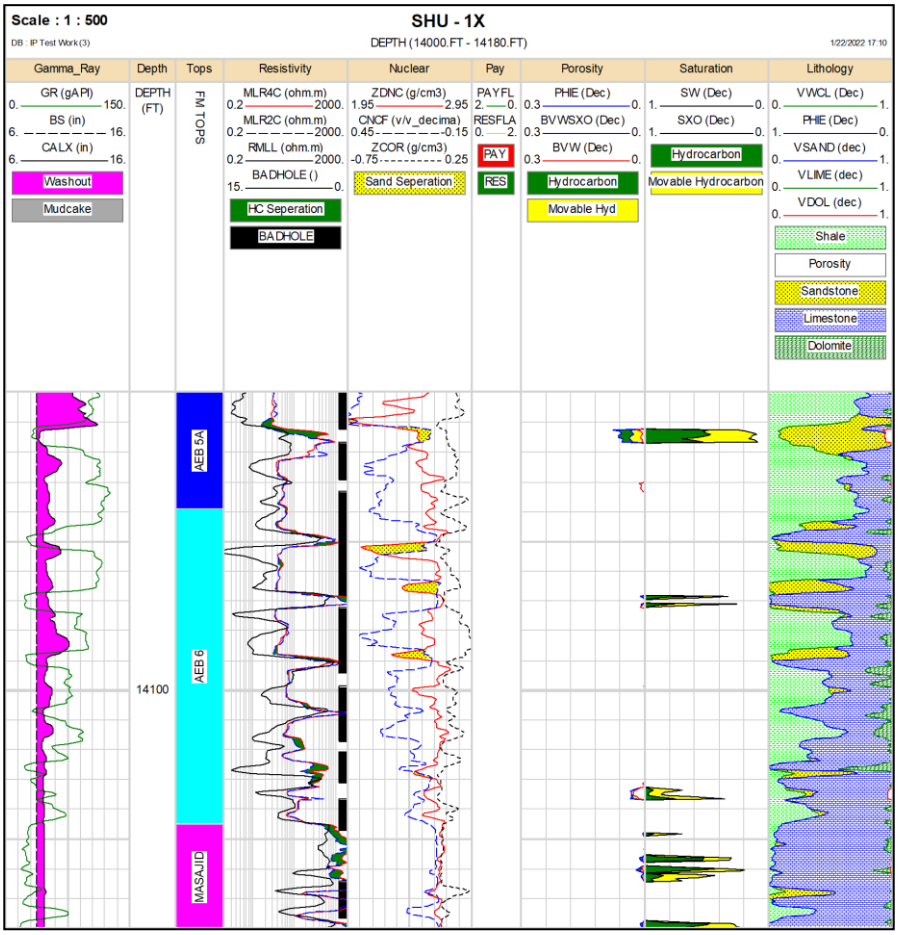

Fig.15. Litho-Saturation Crossplot of AEB-6 unit in SHU-1X well.

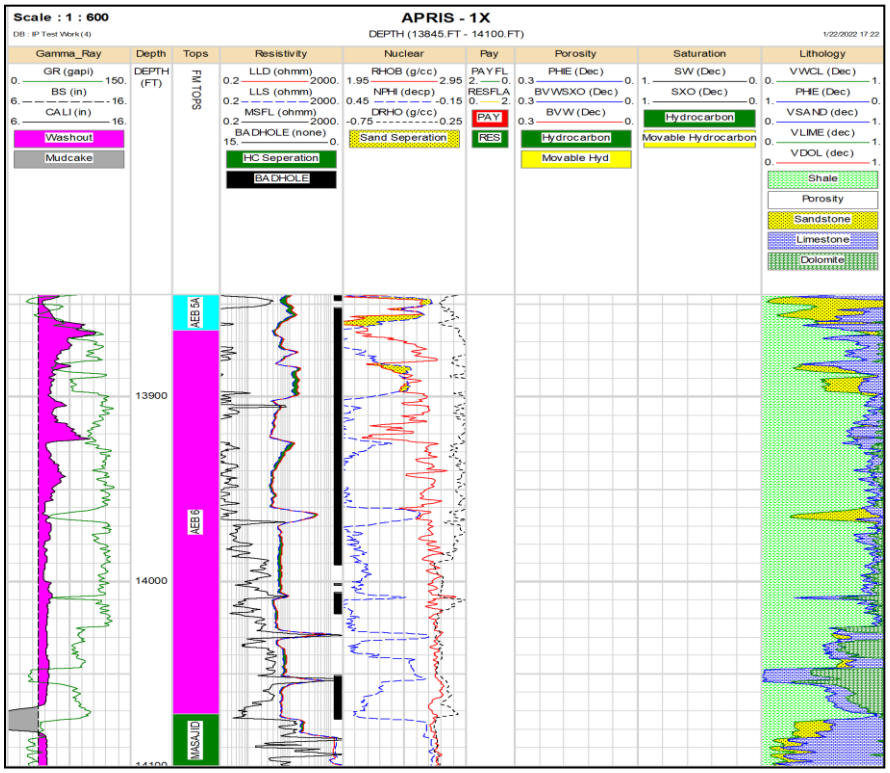

Fig.16. Litho-Saturation Crossplot of AEB-6 unit in APRIES-1X well.

Table 1: Matrix densities of common lithologies constants used in the density porosity formula **(after Schlumberger, 1972)**.

Rocks	ρ_{ma} (gm/cc)
Sandstone	2.648
Limestone	2.710
Dolomite	2.876
Anhydrite	2.977
Salt	2.032

Table. 2: Petrophysical results of AEB-3D reservoir unit in the studied wells.

Well Name	Reservoir Name	Gross thickness (ft)	Gross sand (ft)	Net pay (ft)	Net / Gross (%)	V_{sh} (%)	Φ_{eff} (%)	S_w (%)	S_h (%)
GEB – 1X	AEB-3D	162	3.25	0	0	3	9.5	70	30
GEB – 2X		54	7	0	0	80	0	100	0
SHU – 1X		136	46.5	13	28	4	8.8	38	62
APRIES – 1X		153	8	7	87.5	4.4	9	65	35

Table. 3: Petrophysical results of AEB-3G reservoir unit in the studied wells.

Well Name	Reservoir Name	Gross thickness (ft)	Gross sand (ft)	Net pay (ft)	Net / Gross (%)	V_{sh} (%)	Φ_{eff} (%)	S_w (%)	S_h (%)
GEB – 1X	AEB-3G	Faulted							
GEB – 2X		104	38	5	13	6.1	7.5	41.5	58.5
SHU – 1X		50	6.5	5	77	1.7	9.3	30	70
APRIES – 1X		167	30	0	0	4	8	76	24

Table. 4: Petrophysical results of AEB-6 reservoir unit in the studied wells.

Well Name	Reservoir Name	Gross thickness (ft)	Gross sand (ft)	Net pay (ft)	Net / Gross (%)	V_{sh} (%)	Φ_{eff} (%)	S_w (%)	S_h (%)
GEB – 1X	AEB-6	402	22.75	12.5	55	5.3	8.8	25.5	74.5
GEB – 2X		223	8	7	87.5	7.5	7.5	13.3	86.7
SHU – 1X		196	0	0	0	65	0	100	0
APRIES – 1X		220	7	0	0	90	0	100	0

التقييم البتروفيزيقي باستخدام تسجيلات الآبار في خزانات علم البويب، بحوض شوشان، شمال الصحراء الغربية، مصر

إبراهيم عثمان[١]، عبد العزيز عبد الدايم[١]، محمد رفعت سليمان[١]، جاد القاضي[٢]

[١]قسم الجيولوجيا، كلية العلوم، جامعة طنطا، طنطا، ٣١٥٢٧، مصر

[٢]المعهد القومي للبحوث الفلكية والجيوفيزيقية، حلوان، مصر

تم إجراء التحليل البتروفيزيقي لبعض وحدات خزان علم البويب بعصر الطباشيري السفلي باستخدام تسجيلات آبار من أربعة آبار تقع في الجزء الغربي من حوض شوشان، شمال الصحراء الغربية، مصر. تم حساب العديد من الخصائص البتروفيزيقية للخزانات المدروسة، والتي تشمل حجم صخور الطفلة (V_{SH})، والمسامية الكلية والفعالة (PHI_T و PHI_E)، ودرجة تشبعها بالماء (S_W)، ودرجة تشبعها بالهيدروكربونات (S_H). أوضح تفسير التوقيعات المتقاطعة لقيم تسجيلات النيوترونات والكثافة والتسجيلات الصوتية، إلى أن الحجر الرملي هو المكون الرئيسي لصخور الخزانات مع بعض صخور الكربونات في بعض الوحدات الصخرية. علاوة على ذلك، أشارت تحليلات نتائج التشبع لصخور الخزانات إلى وجود نطاقات هيدروكربونية، والتي ترتبط بشكل أساسي بصخور الحجر الرملي التي تتميز بمحتواها المنخفض من الطفلة، لأن وجودها يضر بجودة الخزان؛ حيث تسد المسام، وتقلل من تخزين وتدفق الهيدروكربونات. يوضح تحليل البيانات البتروفيزيقية أن الوحدات الصخرية المدروسة تتميز بنوعية خزانات جيدة، حيث ان لها قيم مسامية فعالة تتراوح بين ٨ و ١٠٪ بمتوسط ٩٪ وقيم تشبعها بالمياه منخفضة أقل من ٣٥٪. وجد أن نطاقات الخزان الأكثر احتمالية لتواجد الهيدروكربونات موجودة في الجزء العلوي والمتوسط داخل وحدات الخزانات والتي يوصى بها عند حفر آبار للاستكشاف والانتاج في المستقبل.